Global Registration of 3D Cerebral Vessels to Its 2D Projections by a New Branch-and-Bound Algorithm

Kexue Fu, Yinlong Liu, and Manning Wang, *Member, IEEE*

***Abstract*—Endovascular interventions are usually guided by intraoperative 2D images, which cannot fully reflect the 3D structure of vessels and sometimes cause ambiguity. Registering preoperative 3D images to intraoperative 2D images can help eliminate this ambiguity. Most existing methods can only converge to a local optimal solution. Similar to POSE [1], we formulate the problem as 2D-3D point set registration, and develop a fast and accurate global registration method. We propose a novel objective function using consensus set between the 3D points and the projection lines of the 2D points in the 3D space, and introduce a new global optimal rotation search algorithm. The translation search problem is tackled by synchronized grid search in the translation space. Furthermore, we extend the algorithm to register 3D vessels to its two projections, which only increases the runtime slightly but improves the 3D registration accuracy significantly. The proposed method is approximately two times faster than POSE. Experiments on real data show that the mean 3D rotation error is reduced from 5.55 degrees of POSE to 1.62 degrees and the mean translation error is reduced from 8.60 mm of POSE to 1.06 mm by the proposed double-plane method.**

***Index Terms*—Branch-and-bound, geometric bound, global optimization, point set registration, vessel registration.**

I. Introduction

CEREBROVASCULAR diseases are the leading cause of disability and death worldwide [2]–[4]. With the development of computers and medical imaging technology, many cerebrovascular diseases are currently treated with endovascular image-guided interventions (EIGIs) [5], [6], such as ischaemic stroke, carotid and intracranial stenosis, intracranial aneurysms, and so on. In EIGI, clinicians use catheters or microcatheters to deliver drugs and devices along blood vessels to designated locations. EIGI can help achieve less invasive, more precise treatment, and leads to less complications and higher survival rate [7], [8]. Essentially, EIGI utilizes intraoperative 2D images to guide the catheters. However, the fusion of 2D and 3D anatomical information is an essential part of EIGI [5]. In order to achieve this kind of information fusion, clinicians should observe not only 2D images, but also 3D images. Usually, the 3D images, such as Computed Tomography Angiography (CTA), are acquired and displayed to the clinicians just before the start of EIGI. The 2D images, such as Digital Subtraction Angiography (DSA), are acquired during EIGI. In traditional EIGI procedures, clinicians can only cognitively fuse the 2D and 3D images in their mind, but this process relies severely on the experience of clinicians. Therefore, an automatic and accurate method to register the 2D and 3D images is highly demanded.

Registering 2D and 3D medical images is to estimate a transformation of the 3D images to make it align with the human body in the 2D imaging coordinate system when the 2D images are taken [9]. This is usually done by optimizing an objective function defined on the 2D image plane. There are many researches on 2D-3D medical image registration in literature, and they can be roughly classified into two categories according to how the objective function is defined. The first category maximizes the similarity between the original 2D images and the 2D images generated from the 3D images by Digital Radiography Reconstruction (DRR) [10]–[12]. These methods are easy to fall into local optimal solution and suffer from high computational cost [5]. The second category extracts vessels from images and transform 2D-3D image registration into the registration of point sets representing the vessel centerlines [13]–[16], as illustrated in Fig. 1. Here, the 3D vessels are assumed to experience only rigid transformation. Some other vessels may experience fairly large non-rigid deformation between 2D and 3D images during registration [17], such as vessels in heart and liver, but the non-rigid deformation of cerebral vessels is small in EIGI because they are embedded in brain that is fixed in the skull fairly steadily. Therefore, many existing studies [12], [18], [19] assume rigid transformation of the 3D vessels in registering 2D and 3D cerebral vessels and we follow this assumption in this study. 2D-3D point set registration is a fundamental problem in computer vision but early methods can only converge to a local optimal solution. Several global 2D-3D point set registration approaches have been proposed [20]–[22], but they are not efficient for 2D-3D vascular registration because of their problem formulation, which parameterize the problem with the pose of the 2D imaging system. A new problem formulation that estimates the rotation and translation of the 3D vessels is given

Manuscript received July 12, 2020; revised December 5, 2020; accepted January 22, 2021. Date of publication January 27, 2021; date of current version February 22, 2021. This article was recommended for publication by Associate Editor P. Poignet and Editor P. Dario upon evaluation of the reviewers' comments. This work was supported in part by the National Natural Science Foundation of China under Grant 62076070. *(Kexue Fu and Yinlong Liu are co-first authors.) (Corresponding author: Manning Wang.)*

Kexue Fu and Manning Wang are with the Digital Medical Research Center, School of Basic Medical Science, Fudan University, Shanghai 200032, China, and also with the Shanghai Key Laboratory of Medical Image Computing and Computer Assisted Intervention, Fudan University, Shanghai 200032, China (e-mail: kxfu18@fudan.edu.cn; mnwang@fudan.edu.cn).

Yinlong Liu was with the Digital Medical Research Center, School of Basic Medical Science, Fudan University, Shanghai 200032, China. He is now with the Department of Informatics, Technical University of Munich, 80333 Munich, Germany (e-mail: yinlong.liu@tum.de).

Digital Object Identifier 10.1109/TMRB.2021.3055020

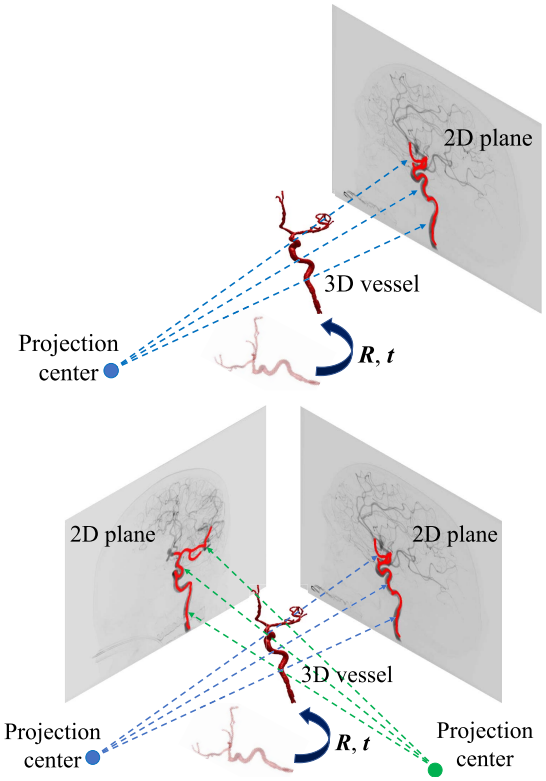

Fig. 1. Illustration of registering 3D vessels to its one (top) or two (bottom) projections. The objective is to find a rotation $\boldsymbol{R}$ and a translation $\boldsymbol{t}$ of the 3D vessels so that its projection aligns with the vessels on one or two 2D planes. The projection parameters are assumed to be known.

in POSE [1], and a Branch-and-Bound (BnB) based global rotation search algorithm is proposed. Recently, deep learning techniques have also been used to register 3D CT image to 2D X-ray images [23], [24], but they have the problems of data dependence and poor generalization ability.

In this article, we propose a novel global algorithm to register 3D vessels to its one or two 2D projections. We utilize the same problem formulation as in [1], but we propose a new 3D geometric bound, which is tighter and more efficient than the bound used in [1]. The algorithm guarantees global optimality in searching 3D rotation by utilizing BnB and the proposed bound, and synchronized multi-start grid search is utilized to search the 3D translation efficiently. In addition, we develop a two-step search method to register 3D vessels to its two projections with a slight increase of time but a large improvement of accuracy. Experiments on synthetic and real data show that the proposed algorithm significantly outperforms state-of-the-art local and global methods in terms of both speed and accuracy.

II. Related Work

Cerebral vessels experience little non-rigid deformation during EIGI [5], so we only review the 2D-3D medical image registration methods, in which the 3D images undergo rigid transformation. These methods can be roughly divided into three categories: intensity-based methods, centerline-based methods and deep learning methods.

A. Intensity-Based 2D–3D Registration Methods

The intensity-based methods generate synthetic 2D projection images with respect to a rigid transformation of the 3D image and measure the similarity between the synthetic 2D image and the real 2D image, such as [10]–[12], [18], [25], [26]. The Similarity Measures (SM) often used are mutual information, cross correlation, pattern intensity, gradient correlation and gradient difference. Hipwell *et al.* analyzed six different SMs, and used gradient difference and pattern intensity to obtain the best results of brain MRA and 2D-DSA registration [12]. Ruijters *et al.* used the dot-product of the two images as the SM to register the 2D distance transform of a projected skeleton of the 3D image with the 2D fluoroscopy image of vessels [25]. The major problem of this approach is that DRR usually suffers from high computational cost. Several intensity-based hybrid methods have been proposed to avoid the high computational cost of DDR. For example, Jomier *et al.* projected 3D vascular centerline onto 2D-DSA, and smoothed the intensity near the projection point in proportion to the corresponding vascular radius [27]. The SM is the sum of the smooth intensity weighted by the radius of the corresponding vessel. Nevertheless, the intensity-based methods can only converge to a local optimal solution, and the convergence basin is usually small, which affects the accuracy of theses methods and makes them difficult to initialize.

B. Centerline-Based 2D–3D Registration Methods

The centerline-based methods represent the vessels with centerline points and formulate the problem as 2D-3D point set registration, which is then tackled by point set registration techniques, such as Iterative Closest Point (ICP) [28] and probability distribution based methods [14]. For example, Feldmar *et al.* used ICP to register 3D vessels from MRA to 2D vessels from X-ray [13]. Groher *et al.* proposed a two-step optimization method based on a modified ICP framework to register liver vessels from 3D CTA and 2D DSA images [29]. Similar to intensity-based approaches, ICP also only converges to a local optimal solution and the convergence basin is small, so a good initialization is needed to achieve accurate registration. The small convergence basin is mainly due to the hard one-to-one point correspondence utilized in ICP, so soft correspondence approaches, including one-to-many correspondence explored in SoftPosit [16] or modeling the point set as Gaussian Mixture Models (GMM) [14], are utilized to enlarge the convergence basin. However, these methods are still locally optimal, and it is difficult for them to find an acceptable registration result without a good initialization.

To achieve global registration, Khoo and Kapoor modeled 2D-3D vessel registration as semidefinite programing that can be globally solved [30]. However, global optimality can only be achieved when the position of the points is noiseless, which is unrealistic in real applications. Liu *et al.* proposed a BnB-based method of 2D-3D point set registration, named POSE, but they only register the 3D points to one 2D projection [1]. In addition, their geometric bound on the 2D plane is loose and complex to calculate, which affects the efficiency of this

method. There are some other works in the computer vision field [20]–[22], but they formulate 2D-3D point set registration as a camera pose estimation problem, and it is not efficient to use them for 2D-3D vessel registration. The reason is that if we want to cover the whole relative angle between the 3D points and the 2D imaging device, we need to move the camera center all around the 3D points, and the range of the translation that needs to be searched is very large [1].

C. Learning-Based Methods

With the rapid development of deep learning, it is also used in registering 2D and 3D medical images. Chou *et al.* trained linear regressors to estimate the rigid transformation parameters of 3D image by minimizing the residual between its DRR and X-ray image [23]. However, linear regressors cannot effectively fit the highly nonlinear mapping from residual to transformation parameters. Therefore, the initial transformation range is only within $\pm 2^\circ$ and $\pm$ 5cm. Liao *et al.* proposed a deep neural network for tracking and triangulating interest points to solve the problem of multiview 2D-3D registration, but the trained network can only be used to solve the registration problem between lung CT image and X-ray image [24]. The best mean projected distance is 8.12mm, and the mean target registration error is between 4mm and 10mm. In vessel registration problem, we need new data sets to retrain the network. Most importantly, this method cannot be used when there is only one 2D image. Despite big success in many image processing tasks, deep learning methods still have big limitations in generalization, stability, and accuracy in 2D-3D medical image registration.

Contribution: The main contribution of this article can be summarized as follows.

1) We propose a new objective function and a new 3D geometric bound for global 2D-3D point set registration under the formulation of estimating the rigid transformation of the 3D point set. Global optimal rotation search is achieved by utilizing BnB optimization with the proposed bound, and global translation search is performed by synchronized grid search as in [1]. This method is faster than existing global method because the 3D geometric bound is tighter and avoids the repeated projection of 3D point on the 2D image plane.

2) We propose a novel two-step searching method to register 3D vessels to its two projections. It can achieve much higher registration accuracy with very little computational overhead. Experiments on both synthetic and real clinical cerebral EIGI data show that our method is faster and more accurate than existing local and global methods.

III. Methods

A. Problem Formulation

As shown in Fig. 1, registration of 3D and 2D vessels is defined as finding a rotation $\boldsymbol{R}$ and a translation $\boldsymbol{t}$ of the 3D vessels so that its projections align with the 2D vessels on one or two projection planes. We formulate the problem as 2D-3D point set registration, where the point set are the centerline points of the vessels. We start from the 2D-3D point set registration problem with a single 2D plane. Let $\mathcal{X} = \{\boldsymbol{x}_i\}_{i=1}^{M}$ and

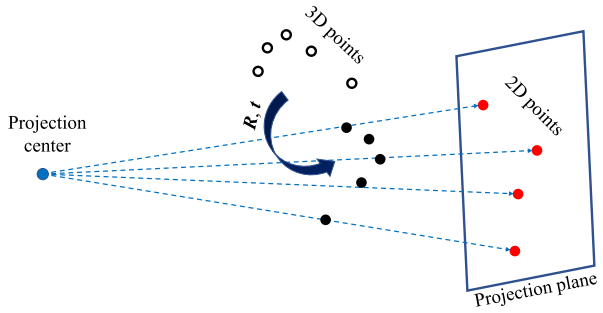

Fig. 2. Illustration of the definition of the objective function for 2D-3D point set registration problem. The objective is to find the best rotation $\boldsymbol{R}$ and translation $\boldsymbol{t}$ to transform the 3D points (hollow black balls before transformation and solid black balls after transformation), so that they form the largest consensus set with the projection lines connecting the projection center and the 2D points (red balls).

$\mathcal{Y} = \{\boldsymbol{y}_j\}_{j=1}^{N}$ represent the 3D and 2D point sets, respectively, where $\boldsymbol{x}_i \in \mathcal{R}^3$, $\boldsymbol{y}_j \in \mathcal{R}^2$. M and N are the number of 3D and 2D points, respectively.

In this article, we use the objective function defined in the 3D space. As shown in Fig. 2, we connect the projection center with each 2D point to form a set of projection lines, and count the consensus pairs between these lines and the 3D points as the objective function. Formally, our goal is to find the best $\boldsymbol{R} \in \mathrm{SO}(3)$ and $\boldsymbol{t} \in \mathcal{R}^3$ that maximize

$$Q(\boldsymbol{R}, \boldsymbol{t}) = \sum_{i=1}^{M} \max_{j=1\cdots N} \left\lfloor Dist\left(\boldsymbol{R}(\boldsymbol{x}_i - \boldsymbol{x}_o) + \boldsymbol{x}_o + \boldsymbol{t}, \overrightarrow{\boldsymbol{y}_j}\right) \le \epsilon_i \right\rfloor \tag{1}$$

where $\boldsymbol{x}_o \in \mathcal{R}^3$ is a predefined rotation center, $\overrightarrow{\boldsymbol{y}_j}$ represents the projection line of $\boldsymbol{y}_j$, $Dist(\bullet, \bullet)$ calculates line-point distance, $\lfloor \bullet \rfloor$ returns 1 if the inner condition is true and 0 otherwise, and ϵ_i is the inlier threshold of the i-th 3D point. In (1), a 3D point $\boldsymbol{x}_i$ is first rotated by $\boldsymbol{R}$ and translated by $\boldsymbol{t}$ to a new position, and then it is checked with every projection line to see if a consensus pair can be formed.

Please note that we use different inlier thresholds for different 3D points in (1), and the inlier threshold is calculated by

$$\epsilon_i = \frac{\epsilon_{2D}}{f} * \left| \boldsymbol{x}_i^z - \boldsymbol{S}^z \right| \tag{2}$$

where $|\bullet|$ is absolute value function, $\boldsymbol{x}_i^z$ is the z-axis coordinate value of the original i-th 3D point after rotation, $\boldsymbol{S}^z$ is the z-axis coordinate value of projection center, f is the distance from projection center to the projection plane, and ϵ_{2D} is the inlier threshold on the 2D plane and it is the same for all the 3D points. The effect of using the inlier threshold calculated by (2) is to use the same inlier threshold of distance on the 2D projection plane. Of course, it is possible to use the same inlier threshold for all 3D points.

B. SO(3) Searching

We start by only considering rotation of the 3D points, and the objective function (1) becomes

$$Q(\boldsymbol{R}) = \sum_{i=1}^{M} \max_{j=1\cdots N} \left\lfloor Dist\left(\boldsymbol{R}(\boldsymbol{x}_i - \boldsymbol{x}_o) + \boldsymbol{x}_o, \overrightarrow{\boldsymbol{y}_j}\right) \le \epsilon_i \right\rfloor \tag{3}$$

Algorithm 1: Global Optimal Pose Optimization in SO(3)

Input: 3D point set $\mathcal{X}$, 2D point set $\mathcal{Y}$, inlier threshold ϵ_{2D};
Output: optimal rotation $\boldsymbol{R}^*$ with quality Q^*;

Calculate projection line $\left\{\overrightarrow{\boldsymbol{y}_j}\right\}$ for each 2D point in $\mathcal{Y}$;
Initialize priority queue q, $\mathbb{B}$={[*center* : 0, 0, 0,]*size* : 2π}, Q^*=0, $\boldsymbol{R}^* = \boldsymbol{I}$;
Insert $\mathbb{B}$ with $\bar{Q}(\mathbb{B})$ into q;
while *q is no empty* **do**
  Find priority cube $\mathbb{B}^*$ to maximize $\bar{Q}(\mathbb{B}^*)$ in q;
  Calculate $\boldsymbol{r}$ center of $\mathbb{B}^*$;
  Calculate $Q(\boldsymbol{R_r})$;
  if $Q_{\boldsymbol{r}} > Q^*$ **then**
    $Q^* = Q_{\boldsymbol{r}}$, $\boldsymbol{R}^* = \boldsymbol{R_r}$;
  end
  if $\bar{Q}(\mathbb{B}^*) = Q^*$ **then**
    $\boldsymbol{R}^* = \boldsymbol{R_r}$;
    return;
  end
  Subdivide $\mathbb{B}^*$ into eight sub-cubes $\left\{\mathbb{B}^d\right\}_{d=1}^{8}$;
  for *each* $\mathbb{B}^d$ **do**
    Calculate $\bar{Q}\left(\mathbb{B}^d\right)$;
    if $\bar{Q}\left(\mathbb{B}^d\right) > Q^*$ **then**
      Insert $\mathbb{B}^d$ with priority $\bar{Q}\left(\mathbb{B}^d\right)$ into q;
    end
  end
end

We use the angular-axis representation of rotation, where the direction and norm of a rotation vector $\boldsymbol{r}$ represents the rotation axis and the rotation angle, respectively. Rotation matrix can be calculated from rotation vector through *Rodrigues'*s formula [31]. Therefore, the whole rotation space can be expressed as a ball centered at the origin with a radius π. For the convenience of branching, we use a cube that has a side length of 2π and encloses the ball as the search space of rotation.

We use a typical BnB algorithm to find the globally optimal rotation maximizing (3), which is outlined in **Algorithm** 1. As a BnB-based algorithm, finding a proper upper bound $\bar{Q}(\mathbb{B})$ is the key for **Algorithm** 1, where $\mathbb{B}$ is a cubic branch in the rotation space and $\forall \boldsymbol{R} \in \mathbb{B}$,

$$\max_{R \in \mathbb{B}} Q(\boldsymbol{R}) \leq \bar{Q}(\mathbb{B}) \tag{4}$$

The quality of $\bar{Q}(\mathbb{B})$ determines the performance of the algorithm and we need a $\bar{Q}(\mathbb{B})$ that is not only tight but also easy to calculate.

Before deriving the novel bound, we will first introduce a lemma given in [1] for completeness and easy understanding of the new bound. This lemma gives the geometric bound of a 3D point under an arbitrary rotation in a cubic branch in the rotation space. As shown in Fig. 3(a), when a 3D point is rotated by an arbitrary rotation, it falls on a sphere centered at the rotation center, and when the rotation is confined in a cubic branch of the rotation space, the rotated point is confined in a small ball, which is called uncertainty ball.

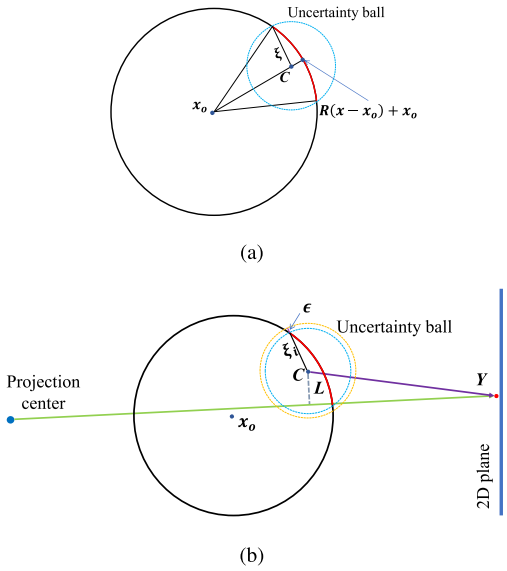

Fig. 3. (a) 2D illustration of uncertainty ball. (b) Illustration of consensus pair checking. When the distance between a projection line (green) and the center of the uncertainty ball of a 3D point is no greater than the inlier threshold ϵ, the projection line and the 3D point form a consensus pair.

Lemma 1: Given a 3D point $\boldsymbol{x} \in \mathcal{R}^3$, the rotation center $\boldsymbol{x}_o$, and a cubic rotation branch $\mathbb{B}$, let $\boldsymbol{p}$ and $\boldsymbol{q}$ be the points at two opposite corners of $\mathbb{B}$, then the center of $\mathbb{B}$ is $\boldsymbol{c} = 0.5*(\boldsymbol{p}+\boldsymbol{q})$. For $\forall \boldsymbol{R}_u \in \mathbb{B}$, $\boldsymbol{x}_u = \boldsymbol{R}_u(\boldsymbol{x} - \boldsymbol{x}_o) + \boldsymbol{x}_o$ we have

$$\|\boldsymbol{x}_u - \boldsymbol{C}\| \leq \xi \tag{5}$$

This Lemma means the rotated point falls in a ball centered at $\boldsymbol{C}$ with a radius of ξ, whose calculation method can be found in [1]. Then we give the following lemma for the derivation of the novel bound proposed in this article.

Given a 3D point $\boldsymbol{x} \in \mathcal{R}^3$, the rotation center $\boldsymbol{x}_o$. For $\forall \boldsymbol{R}_u \in \mathbb{B}$ we have

$$\boldsymbol{R}_u(\boldsymbol{x} - \boldsymbol{x_o}) + \boldsymbol{x_o} \in \text{ Ball} \tag{6}$$

where Ball represents the uncertainty ball in Fig. 3.

In the previous study [1], the uncertainty ball was projected onto the 2D plane to search consensus pair with the 2D points, which brought two disadvantages. First, as shown in [1], the projection, which is an ellipse, is expanded to a circle that encloses the ellipse as the new geometric bound for easier consensus pair detection, but the expansion loosens the bound because the circle is larger and may form more consensus pairs with the 2D points on the projection plane. Second, as given in [1], the calculation of both the projected ellipse and the enclosing circle is fairly complicated, and the calculation must be done for each 3D point. To avoid these two disadvantages, we propose to calculate the upper bound in 3D space. As illustrated in Fig. 3(b), we check whether a projection line and the uncertainty ball of a rotated 3D point constitutes a consensus pair, and then count the number of 3D points whose uncertainty ball find a consensus line as the upper bound. The upper bound is summarized as follows.

For a rotation cube $\mathbb{B}$ with center rotation $\boldsymbol{R}_c$, in the parameter space of SO(3), we define the following function:

$$\bar{Q}(\mathbb{B}) = \sum_{i=1}^{M} \max_{j=1\cdots N} \left\lfloor Dist\left(\boldsymbol{R}_c(\boldsymbol{x}_i - \boldsymbol{x}_o) + \boldsymbol{x}_o, \overrightarrow{\boldsymbol{y}_j}\right) \le \epsilon_i + \xi_i \right\rfloor \tag{7}$$

where ξ_i is the radius of the uncertainty ball of $\boldsymbol{x}_i$ under an arbitrary rotation in $\mathbb{B}$. We have the following theorem.

Theorem 1: For any cubic rotation branch $\mathbb{B}$, $\forall \boldsymbol{R} \in \mathbb{B}$, we define

$$\max_{\boldsymbol{R}\in\mathbb{B}} Q(\boldsymbol{R}) \le \bar{Q}(\mathbb{B}). \tag{8}$$

Proof: For any 3D point $\boldsymbol{x}_i$, the projection line $\overrightarrow{\boldsymbol{y}_j}$ of any 2D point $\boldsymbol{y}_j$, a rotation cube $\mathbb{B}$ with center rotation $\boldsymbol{R}_c$, and $\forall \boldsymbol{R}_u \in \mathbb{B}$ we define

$$(\boldsymbol{x}_i)_u = \boldsymbol{R}_u(\boldsymbol{x}_i - \boldsymbol{x}_o) + \boldsymbol{x}_o$$
$$(\boldsymbol{x}_i)_c = \boldsymbol{R}_c(\boldsymbol{x}_i - \boldsymbol{x}_o) + \boldsymbol{x}_o$$

From *Lemma* 1, we know that a point will fall within a uncertainty ball after being rotated by an arbitrary rotation $\boldsymbol{R}_u \in \mathbb{B}$. The distance from any point in the uncertainty ball to the line $\overrightarrow{\boldsymbol{y}_j}$ must be greater than or equal to the distance from the uncertainty ball to the line, as shown in Fig. 3.

$$\mathrm{Dist}\left((\boldsymbol{x}_i)_c, \overrightarrow{\boldsymbol{y}_j}\right) - \xi_i \le \mathrm{Dist}\left((\boldsymbol{x}_i)_u, \overrightarrow{\boldsymbol{y}_j}\right)$$

where $\mathrm{Dist}((\boldsymbol{x}_i)_c, \overrightarrow{\boldsymbol{y}_j}) - \xi_i$ equals the distance from the uncertainty ball to $\overrightarrow{\boldsymbol{y}_j}$. Furthermore, the objective function value of any rotation $\boldsymbol{R}_u$ and the upper bound of a rotation cube $\mathbb{B}$ can be expressed as follows:

$$Q(\boldsymbol{R}_u) = \sum_{i=1}^{M} \max_{j=1\cdots N} \left\lfloor Dist\left((\boldsymbol{x}_i)_u, \overrightarrow{\boldsymbol{y}_j}\right) \le \epsilon_i \right\rfloor$$
$$\bar{Q}(\mathbb{B}) = \sum_{i=1}^{M} \max_{j=1\cdots N} \left\lfloor Dist\left((\boldsymbol{x}_i)_c, \overrightarrow{\boldsymbol{y}_j}\right) \le \epsilon_i + \xi_i \right\rfloor$$
$$\therefore \max_{\boldsymbol{R}\in\mathbb{B}} Q(\boldsymbol{R}) \le \bar{Q}(\mathbb{B}).$$

■

C. SE(3) Searching

We extend our method in SO(3) space to SE(3) space, which is defined by (9). We adopt the synchronized multi-start grid search scheme [1] in the translation space, which is much more efficient than joint search of the rotation and translation. The whole process can be summarized as **Algorithm** 2 and **Algorithm** 3.

$$\mathrm{SE(3)} = \left\{ \boldsymbol{T} = \begin{bmatrix} \boldsymbol{R} & \boldsymbol{t} \\ \boldsymbol{0}^T & 1 \end{bmatrix} \in \mathcal{R}^{4\times4} \right\}. \tag{9}$$

D. Fast Double-Plane Registration Method

Our experiment shows that there is a large translation error in the projection direction when registering 3D vessels to one 2D projection, and the problem can be well addressed by registering the 3D vessels to its two projections with different projection directions. Here, we adopt a simple two-step registration method. As shown in Fig. 4, we first run **Algorithm** 2 to register the 3D vessels to its one projection in the first step. We empirically find that after registering 3D vessels to the first 2D projection plane, there may be a moderate translation error in the 3D space along the projection direction. This is because when the 3D vessels move slightly away from its ground truth position along the projection direction, the value of the objective function, which is defined on the base of consensus set, may keep unchanged. However, this kind of translation may cause big projection error on the other projection plane, as illustrated in Fig. 4. Therefore, the 3D translation error can be effectively reduced by moving the 3D vessels along the projection direction of the first plane and make its projection on the second plane align with the 2D vessels on it. This is achieved by a one dimensional grid

Algorithm 2: Global Pose Optimization in SE(3)

Input: 3D point set $\mathcal{X}$, 2D point set $\mathcal{Y}$, inlier threshold ϵ_{2D}, translational cube $\mathbb{V}$;
Output: optimal rotation $\boldsymbol{R}^*$ and translation $\boldsymbol{t}^*$ with quality E^*;

Subdivide $\mathbb{V}$ into $\{\mathbb{V}_h\}_{h=1}^k$ and the center of each cube $\{\boldsymbol{t}_h\}_{h=1}^k$;
Initialize $\{E_h^*\}_{h=1}^k = 0$, $E^* = 0$, $\{\bar{E}(\mathbb{B}_h, \boldsymbol{t}_h)\}_{h=1}^k = M$, global upper bound $\hat{E} = M$, $\{\mathbb{B}_h\}_{h=1}^k = \{[center : 0, 0, 0], size : 2\pi\}$, $\{\boldsymbol{R}_h^*\}_{h=1}^k = \boldsymbol{I}$, translation branch search flag $\{F_h\}_{h=1}^k$=1, stop flag $\{S_h\}_{h=1}^k$=0;
Calculate projection line $\left\{\overrightarrow{\boldsymbol{y}_j}\right\}$ for 2D point set $\mathcal{Y}$;
Insert $\{\mathbb{B}_h\}_{h=1}^k$ with $\{\bar{E}(\mathbb{B}_h, \boldsymbol{t}_h)\}_{h=1}^k$ into $\{q_h\}_{h=1}^k$;
while *1* **do**
  for *each center of translational cube* **do**
    if *size*$(\mathbb{B}_h) > 0$ **then**
      Input $\mathcal{Y}$, $\mathcal{X}$, ϵ, $\boldsymbol{t}_h$, $\mathbb{B}_h$, $\hat{E}$, E_h^*, E^*, $\boldsymbol{R}_h^*$, F_h;
      Go into **Algorithm 3**;
      Output $\boldsymbol{R}_h^*$, $\mathbb{B}_h$, S_h, E_h^*, $\bar{E}(\mathbb{B}_h, \boldsymbol{t}_h)$, F_h;
    end
    if *sum*$(\{S_h\}_{h=1}^k) > 0$ **then**
      Find where $\{S_h\}_{h=1}^k == 1$;
      $\boldsymbol{R}^* = \boldsymbol{R}_h^*$, $\boldsymbol{t}^* = \boldsymbol{t}_h^*$;
      return;
    end
    $\hat{E} = \max(\{\bar{E}(\mathbb{B}_h, \boldsymbol{t}_h)\}_{h=1}^k)$;
    $E^* = max(E_h^*)$;
  end
end

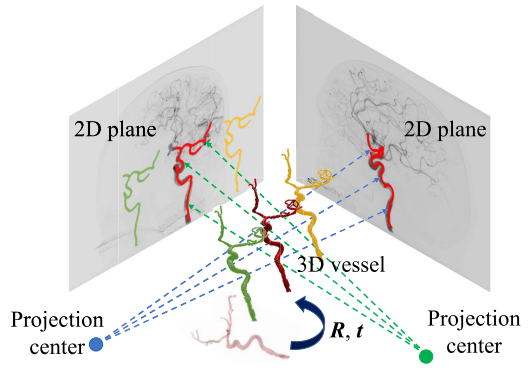

Fig. 4. Illustration of two-step double-plane registration method.

Algorithm 3: Update a Solution in SO(3)

Input: 3D point set $\mathcal{X}$, set of projection lines $\left\{\overrightarrow{\boldsymbol{y}}_j\right\}$, inlier threshold ϵ_{2D}, center of each cube $\boldsymbol{t}_h$, rotation cube set $\mathbb{B}_h$, upper bound of $\boldsymbol{t}_h \rightarrow \bar{E}(\mathbb{B}_h, \boldsymbol{t}_h)$, each upper bound E_h^*, optimal upper bound E^*, optimal rotation $\boldsymbol{R}_h^*$, translation branch search flag F_h;

Output: optimal rotation $\boldsymbol{R}_h^*$ at $\boldsymbol{t}_h$, rotation cube set $\mathbb{B}_h$, stop flag S_h, each upper bound E_h^*, upper bound of $\boldsymbol{t}_h \rightarrow \bar{E}(\mathbb{B}_h, \boldsymbol{t}_h)$, translation branch search flag F_h;

Initialize $S_h = 0$, discard the upper bound less than E^* in $\mathbb{B}_h$;
if $\mathbb{B}_h$ *is empty* **then**
  $\boldsymbol{R}_h^* = \emptyset$, $\mathbb{B}_h = \emptyset$, $\bar{E}(\mathbb{B}_h, \boldsymbol{t}_h) = 0$, $E_h^* = 0$;
  return;
end
Find highest priority cube $\mathbb{B}_h^*$ in $\mathbb{B}_h$;
if $F_h = 1$ **then**
  Calculate center $\boldsymbol{r}$ of $\mathbb{B}_h^*$;
  Calculate $Q(\boldsymbol{R_r})$;
  if $Q_{\boldsymbol{r}} > E_h^*$ **then**
    $E_h^* = Q_{\boldsymbol{r}}$, $\boldsymbol{R}_h^* = \boldsymbol{R_r}$;
  end
  if $\bar{E}(\mathbb{B}_h, \boldsymbol{t}_h) = E_h^*$ **then**
    if $\bar{E}(\mathbb{B}_h, \boldsymbol{t}_h) = E^*$ **then**
      $S_h = 1$;
    else
      $F_h = 0$;
    end
    return;
  end
  Subdivide $\mathbb{B}_h^*$ into eight $\left\{\mathbb{B}_h^d\right\}_{d=1}^8$;
  for *each* $\mathbb{B}_h^d$ **do**
    Calculate $\bar{Q}\left(\mathbb{B}_h^d\right)$, insert $\bar{Q}\left(\mathbb{B}_h^d\right)$ into $\mathbb{B}_h$;
  end
else
  if $\bar{E}(\mathbb{B}_h, \boldsymbol{t}_h) = E^*$ **then**
    $S_h = 1$;
    return;
  end
end

search on the projection direction of the first plane in the second step. Concretely, we select a one dimensional translation search range along the projection direction of the first plane and make the search range centered at the registered position of the 3D vessels. In the search range, we sample h test positions with equal interval and move the 3D vessels to each position. The same objective function as used in registering to the first projection plane is evaluated at each test position with respect to the second projection plane, and the test position that results in the maximum objective function value is retained as the result of the second step.

IV. Experiments and Results

In this section, we evaluate the performance of the proposed algorithms and compare them to state-of-the-art algorithms using both synthetic and real clinical data. Our global optimal single-plane 2D-3D point set registration algorithm in the parameter space of SO(3) and SE(3) are denoted as *Our_SO*3*_S* and *Our_SE*3*_S*, and they correspond to **Algorithm** 1 and **Algorithm** 2, respectively. Our double-plane 2D-3D point set registration algorithm in the parameter space of SE(3) is denoted as *Our_SE*3*_D*, which corresponds to the process described in Section III-D.

In synthetic data experiment, we first compared *Our_SO*3*_S* to two typical local methods, SoftPosit [16], GMM and one recent global method POSO [1] on rotation search. In this experiment, we focused on the global optimality and speed of these methods. Then, we studied the robustness of *Our_SE*3*_S* to different levels of noise, 2D and 3D outliers and compare it to SoftPosit, GMM and a recent global method POSE [1]. Finally, we compared the performance of *Our_SE*3*_S* and *Our_SE*3*_D*. In the real data experiment, we compared SoftPosit, GMM, POSE, RANSAC, GOPAC [20], *Our_SE*3*_S* and *Our_SE*3*_D*. We also compare a new double-plane registration method which is obtained by combining POSE with our fast double-plane registration method, and denoted it as POSE+FD. A local refinement by GMM is performed at the end of all global methods and its runtime is added to the total runtime of every global method.

The codes of SoftPosit, GOPAC, POSO and POSE in MATLAB are made available by the authors. GMM is an extension of the 3D-3D point set registration algorithm [14], and we implemented it for 2D-3D point set registration in MATLAB. Our code was implemented in MATLAB2018b. All experiments were run on a PC(*Intel Core i*7 − 7700*K CPU*@4.20GHz ×8) with Ubuntu18.04 LTS operating system.

A. Synthetic Data Experiments

1) Performance Analysis in SO(3): Twenty uniformly distributed random 3D points were generated in a cube of edge size 100 centered at point $(0, 0, 500)$. The projection plane was placed at $(0, 0, 1000)$, and the 3D points were projected to the 2D plane to generate the 2D points. We rotated the 3D points in the range of $[-180, 180]$ with an interval of five degrees. For each rotation angle, we generated 50 rotations around different randomly generated rotation axes and registered the rotated 3D points to the 2D points with each algorithm. For GMM, we experimented on two Gaussian kernels with standard deviation of 5 and 10. For SoftPosit, we set the maximum number of iterations to 100. We used an inlier threshold $\epsilon_{2D} = 1$ for *Our_SO*3*_S* and set the inlier threshold on the 2D plane of POSO as 1. In this synthetic experiment, we knew the true one-to-one correspondence between the 3D points and the 2D points, and we used mean projected distance (mPD) [32] of corresponding points to evaluate different methods. For each algorithm, we recorded its average runtime and success rate in 50 registrations under the same rotation angle (but different, randomly generated rotation axes), where a registration is considered successful if the mPD is less than 1. The success rate and average runtime are shown in Fig. 5 (a) and (b), respectively. The two global methods, *Our_SO*3*_S* and POSO, achieve 100% success rate at all rotation angles, but *Our_SO*3*_S* is approximately three times faster than POSO. Local methods can achieve 100% success rate only when the rotation angle is very small. Fig. 5 (c) illustrates the evolution of the upper bound and the current best function value in

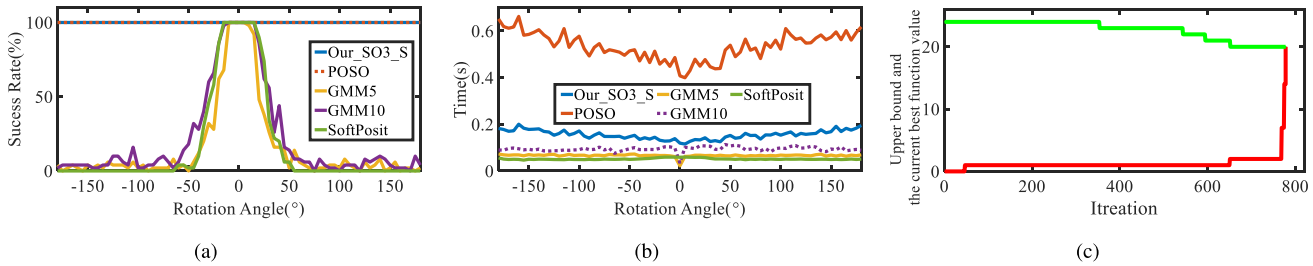

Fig. 5. Results of rotation search experiment using synthetic data. (a) success rate with respect to rotation angle. (b) average runtime with respect to rotation angle. (c) evolution of the upper bound $\bar{Q}$ (green line) and the current best function value Q^* (red line) with respect to iteration.

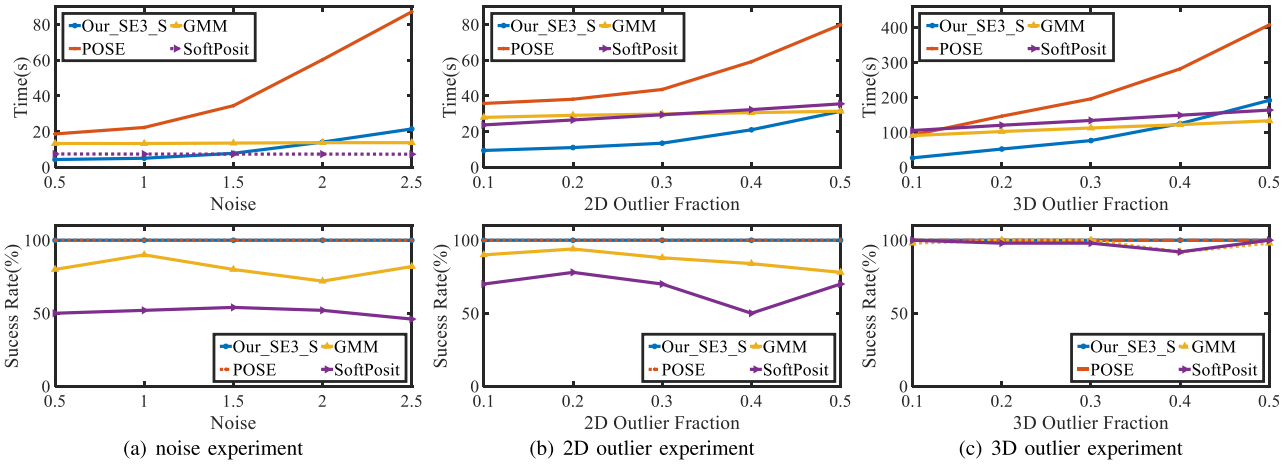

Fig. 6. Average runtime and success rate in 2D-3D point set registration using synthetic data. (a) noise experiment. (b) 2D outlier experiment. (c) 3D outlier experiment.

one registration. In this case of registration, the number of 2D points is 20, and the number of 3D points is 24, out of which four 3D points are outliers. The upper bound starts from 24 and the current best value starts from zero, and they converge at the value of 20, which is the size of the found largest consensus set and also the number of true 2D-3D corresponding point pairs. Our method obtained the global optimal solution after about 800 iterations.

2) Performance Analysis in SE(3): 2D and 3D point sets were first generated in a way similar to the previous section, and the only difference is that a random translation in the range of $[-5, 5]^3$ is used to the 3D points before registration. Both global methods, *Our_SE*3*_S* and POSE, were run by using 27 searching blocks obtained by equally dividing the translation cube along each axis. We used an 2D inlier threshold $\epsilon_{2D} = 5$, for POSE and *Our_SE*3*_S*, and the standard deviation of the GMM algorithm was set to 10. The maximum iteration number of SoftPosit was 100. A registration is considered successful if the registered mPD (distance of corresponding points on the 2D plane) is less than 5.

For the noise experiment, Gaussian noise with standard deviation of 0.5, 1.0, 1.5, 2.0 and 2.5 were added to each coordinate of the 2D points, and for each noise level, 50 registrations with random relative rotation and translation were executed. For a fair comparison, GMM repeated 100 times and SoftPosit repeated 150 times in registering each pair of 2D and 3D points and returned the best result, so that the total runtime of each method in registering a pair of 2D and 3D points is approximately equal to the time of running *Our_SE*3*_S* once. The average runtime and success rate were shown in Fig. 6 (a). Both global algorithms achieved 100% success rate, but *Our_SE*3*_S* is approximately four times faster than POSE. On the contrary, local methods resulted in much lower success rate with approximately equal or longer running time.

For the 2D and 3D outlier experiments, Gaussian noise with a standard deviation of 1 was added to the coordinates of the inlier 2D points. Random outlier points were added to 2D or 3D point set before registration, and the number of outlier points were 0.2, 0.4, 0.6, 0.8 and 1.0 times the inlier points. For the 2D outlier experiment, SoftPosit and GMM were run 400 and 200 times, respectively. For the 3D outlier experiments, SoftPosit and GMM were run 1800 and 600 times, respectively. The average runtime and success rate with respective to outlier ratio of 2D and 3D outliers are shown in Fig. 6(b) and (c), respectively. In both 2D and 3D outlier experiments, the two global methods achieved 100% success rate, and *Our_SE*3*_S* is much faster than POSE. The success rate of the two local methods are low in 2D outlier experiment, but fairly high in 3D outlier experiment.

3) Translation Error Analysis in Single and Double Planes: We also used the same experimental setting as above. For *Our_SE*3*_D*, in the second step of registering to the second projection plane, the search range is $[-5, 5]$ around the registered position and the searching interval is 1. We compare the 3D translation error of *Our_SE*3*_S* and *Our_SE*3*_D*.

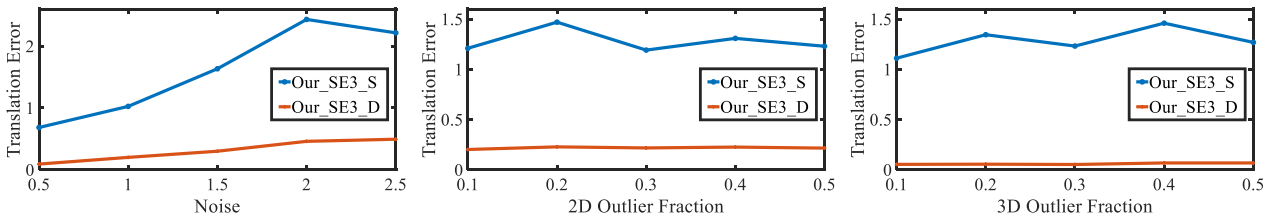

(a) noise experiment (b) 2D outlier experiment (c) 3D outlier experiment

Fig. 7. 3D translation error of *Our_SE3_S* and *Our_SE3_D* registration. (a) noise experiment. (b) 2D outlier experiment. (c) 3D outlier experiment.

TABLE I
RESULTS OF 2D-3D REGISTRATION OF CEREBRAL VESSELS

	Method	Case1	Case2	Case3	Case4	Case5	Case6	Case7	Case8	Case9	Case10	Mean	Std	P-value
Rotation error(°)	RANSAC	123.708	101.589	127.125	131.884	130.752	149.853	124.794	141.420	107.130	129.565	126.782	14.262	< 0.001
	SoftPosit	21.346	16.472	54.116	13.229	22.623	13.820	56.682	14.942	65.759	61.538	34.053	22.323	0.001
	GMM	3.366	5.213	1.605	1.760	6.273	3.030	11.345	10.171	4.193	6.051	5.301	3.301	0.006
	GOPAC	6.549	4.651	10.486	39.799	7.894	3.471	13.440	6.878	129.052	32.244	25.446	38.412	0.215
	POSE	2.399	6.733	0.857	1.762	4.535	2.009	22.879	9.063	**1.184**	4.035	5.545	6.627	0.083
	Our_SE3_S	2.625	4.254	2.231	1.668	**4.532**	1.676	11.994	7.593	1.345	3.590	4.151	3.333	0.036
	POSE+FD	1.907	**1.183**	**0.572**	1.410	5.642	**0.354**	3.219	2.599	1.484	0.459	1.883	**1.612**	0.220
	Our_SE3_D	**1.668**	**1.183**	**0.572**	**0.913**	6.076	**0.354**	**2.894**	**0.638**	1.485	**0.364**	**1.615**	1.746	*
Translation error(mm)	RANSAC	2598.453	2866.033	2891.862	3739.940	2967.329	4895.531	3003.324	2993.898	2551.576	2446.536	3095.448	726.395	< 0.001
	SoftPosit	42.394	88.708	55.209	104.945	71.330	88.693	150.325	51.676	126.791	106.281	88.635	34.577	< 0.001
	GMM	6.301	14.155	3.760	3.530	8.727	10.021	4.625	18.287	11.944	11.339	9.269	4.844	0.001
	GOPAC	92.127	65.519	141.884	286.250	102.136	61.347	173.250	97.963	785.909	244.123	205.051	217.421	0.016
	POSE	7.196	11.170	1.899	3.565	7.402	10.078	14.348	14.295	7.276	8.785	8.601	4.079	< 0.001
	Our_SE3_S	7.128	12.563	2.327	2.691	7.006	9.725	10.008	15.637	9.961	9.830	8.688	4.093	< 0.001
	POSE+FD	**0.829**	**0.834**	**0.846**	**0.993**	**1.578**	**1.243**	1.183	1.073	**0.835**	0.886	**1.030**	**0.246**	0.562
	Our_SE3_D	0.976	**0.834**	**0.846**	1.049	1.974	**1.243**	**1.113**	**0.854**	**0.835**	**0.877**	1.060	0.350	*
TRE(mm)	RANSAC	2393.894	2713.833	2872.587	3991.108	2741.280	4661.019	2992.449	2968.466	2725.604	2364.682	3042.492	725.383	< 0.001
	SoftPosit	36.140	84.050	71.887	117.568	63.087	80.016	136.832	51.068	140.981	98.792	88.042	35.269	< 0.001
	GMM	4.034	12.442	3.626	3.828	11.865	11.246	5.652	16.565	10.384	9.030	8.867	4.417	< 0.001
	GOPAC	33.788	25.548	40.185	54.782	32.968	36.519	25.068	36.600	213.611	103.466	60.253	58.527	0.011
	POSE	6.721	10.476	1.700	3.848	7.063	9.217	12.965	14.038	7.872	8.168	8.207	3.768	< 0.001
	Our_SE3_S	6.692	11.819	2.621	2.931	6.779	9.046	7.999	15.605	10.694	9.370	8.356	**3.933**	< 0.001
	POSE+FD	**0.528**	**0.203**	**0.345**	0.784	**1.438**	**0.664**	**1.477**	1.055	**0.313**	0.566	0.737	**0.452**	0.636
	Our_SE3_D	0.532	**0.203**	**0.345**	**0.749**	1.638	**0.664**	1.561	**0.547**	**0.313**	**0.540**	**0.709**	0.497	*
mPD(pixel)	RANSAC	5.441	5.173	10.069	7.960	6.040	7.021	8.367	7.493	5.681	12.637	7.588	2.338	0.002
	SoftPosit	2.675	2.376	**4.973**	**3.287**	**3.586**	**4.753**	5.180	2.711	**4.747**	4.932	3.922	**1.106**	0.495
	GMM	2.927	1.879	7.585	3.319	4.617	6.069	**3.039**	3.769	6.235	2.178	4.162	1.905	0.002
	GOPAC	2.947	1.678	8.218	3.902	4.949	6.182	3.896	2.733	5.477	2.924	4.291	1.946	0.001
	POSE	**2.206**	1.658	7.172	3.320	3.733	4.972	3.505	2.264	5.703	1.339	3.587	1.879	0.685
	Our_SE3_S	2.208	**1.435**	7.084	3.333	3.712	5.041	3.216	**2.245**	5.756	**1.312**	**3.534**	1.908	0.540
	POSE+FD	2.313	1.483	7.224	3.368	3.764	5.170	3.051	2.458	5.510	1.331	3.567	1.892	0.472
	Our_SE3_D	2.298	1.483	7.224	3.372	3.795	5.170	3.042	2.390	5.510	1.328	3.561	1.898	*
Runtime(s)	RANSAC	4.104	4.021	3.992	4.074	4.064	4.035	4.040	**4.008**	**4.055**	3.917	4.031	**0.052**	0.046
	SoftPosit	5.267	5.224	5.133	5.082	5.117	5.177	4.878	5.151	5.019	4.921	5.097	0.125	0.002
	GMM	4.933	4.937	4.931	5.031	5.673	5.391	4.966	4.820	5.144	4.565	5.039	0.307	0.002
	GOPAC	53.662	53.489	53.798	54.017	54.555	53.764	54.324	54.137	53.903	53.953	53.960	0.316	< 0.001
	POSE	2.641	3.974	2.432	3.434	5.200	3.344	5.112	6.584	6.063	2.585	4.137	1.509	0.001
	Our_SE3_S	**1.316**	2.182	1.662	**1.837**	**3.181**	1.955	2.906	4.531	6.551	1.378	**2.750**	1.658	0.779
	POSE+FD	2.910	3.727	2.328	3.713	5.410	3.306	5.118	6.805	6.195	2.494	4.201	1.578	0.001
	Our_SE3_D	1.524	**1.932**	**1.528**	2.137	3.436	**1.871**	**2.775**	4.405	6.842	**1.247**	2.770	1.733	*

The results are shown in Fig. 7. We can see that 3D translation error is greatly reduced by using the double-plane registration method.

These experiments show that our *Our_SE3_S* is several times faster than POSE, which demonstrate the higher efficiency of the proposed bound. The comparison between *Our_SE3_S* and *Our_SE3_D* shows that the proposed double plane registration method can effectively reduce 3D translation error. In addition, the experiments show that the proposed methods are robust to noise and outliers.

B. Real Data Experiments

We experimented on the cerebral vessel dataset provided in [33], in which one 3D-DSA and two 2D-DSA images of ten patients were provided and the projection parameters and the gold standard registrations were given. In cerebral vascular procedures, the multi-angle 2D-DSA images are taken by a C-arm [34], which is a C-shaped X-ray imaging device that can rotate around the patient's head. We used the method given in [1] to extract centerline points from the original 2D-DSA and 3D-DSA images, and in the last step we used k-means clustering method [35], [36] to cluster 2D point set and 3D point set to 90 points and 60 points, respectively. We followed the method in [1], and generated a random translation in the cube of $[-20, 20]^3$ *mm* and a random rotation in the range of $[-10°, 10°]$. We used an inlier threshold $\epsilon_{2D} = 20$ pixels for POSE, POSE + FD, *Our_SE3_S*, and *Our_SE3_D*. In the second step of registering to the second projection plane, the search range is $[-20, 20]$ *mm* around the registered position and the searching interval is 0.5mm for POSE+FD and *Our_SE3_D*. The standard deviation of the GMM was set to 2 pixels. RANSAC repeated 20,000 times, GMM repeated

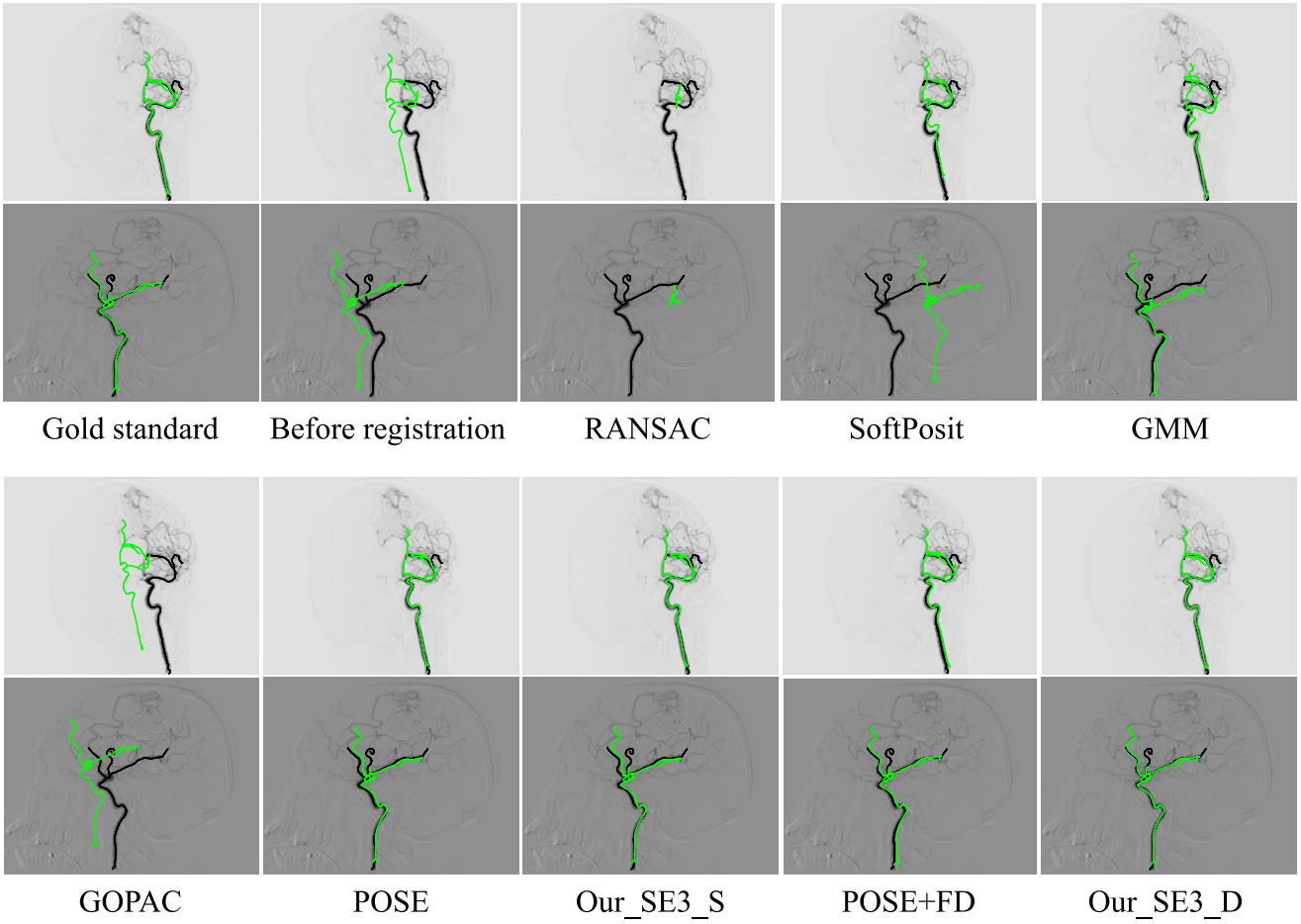

Fig. 8. Visualization of results of case No. 6. The top and the bottom rows are the first and the second projection plane, respectively. Black and green points represent 2D vessel points and projection of 3D vessel points, respectively.

5 times and SoftPosit repeated 10 times so that their total runtime is longer than the proposed methods for each case. Random initialization of translation and rotation in the translation and rotation ranges were used in each run of these two local methods. For GOPAC, we configure the angular tolerance θ by calculating the tangent value of the inlier threshold ϵ_{2D} corresponding to the angle, and set the maximum running time to 50s.

We ran 10 repeated experiments for each case. The 3D rotation and translation error, the mean target registration error (mTRE) [32] of corresponding 3D vessel points, the mPD (we use KNN search to find the nearest point as the corresponding point on the 2D image plane), and the runtime of each case are shown in Table I. After registration with RANSAC, SoftPosit, GMM and GOPAC, there are still large average rotation error and average translation error. The proposed single-plane method *Our_SE*3*_S* is faster than POSE. However, the 3D translation error and mTRE of both methods are large. *Our_SE*3*_D* reduces the translation error, the rotation error and the mTRE, and P-value of paired t-test shows that the improvement is statistically significant. Sometimes *Our_SE*3*_D* even takes less time than *Our_SE*3*_S*, because *Our_SE*3*_D* provides a better initial solution for local refinement, which makes the algorithm converge faster. The experimental results show that after combining with our double-plane registration method, POSE + FD does not significantly increase the registration time of the original method, but can effectively reduce the registration error. POSE + FD and *Our_SE*3*_D* are comparable in accuracy, but *Our_SE*3*_D* is approximately 50% faster. The translation and rotation error in 3D space for the local methods are very large in most cases. In addition, mPD of all eight methods are similar, which indicates that it is not a reliable accuracy measurement in registering 3D vessels to one projection. An illustrative case is shown in Fig. 8.

V. Conclusion

In this article, we propose an efficient global algorithm to solve the 2D-3D vessel registration problem. We first introduce a fast optimal rotation search algorithm for 2D-3D point set registration based on BnB and a novel geometric bound. Then we solve the SE(3) search problem by utilizing synchronized grid search in the translation space. We utilize similar algorithm architecture with POSE [1] for both the SO(3) search and the SE(3) search problem, but our novel bound makes the proposed method approximately two times faster than POSE. In addition, we develop a two-step scheme to register a 3D point set to its two 2D projections, which slightly increase

the runtime but greatly improve the 3D registration accuracy. This technique can be utilized to both POSE and our proposed SE(3) search algorithm, and experiments on real data shows that this two-step technique helps reduce the 3D rotation error from about five degrees to less than 2 degrees, and reduce the 3D translation error from about eight millimeters to about one millimeter. For deformable registration between 3D and 2D vessels, the proposed method can be used for initial coarse registration. Experiments on both synthetic and real clinical data show that the proposed method significantly outperformed state-of-the-art local and global methods.

REFERENCES

[1] Y. Liu, Y. Dong, Z. Song, and M. Wang, "2D–3D point set registration based on global rotation search," *IEEE Trans. Image Process.*, vol. 28, pp. 2599–2613, 2019.

[2] E. Boot, M. S. Ekker, J. Putaala, S. Kittner, F.-E. De Leeuw, and A. M. Tuladhar, "Ischaemic stroke in young adults: A global perspective," *J. Neurol. Neurosurg. Psychiatry*, vol. 91, no. 4, pp. 411–417, 2020.

[3] R. Dong, Z. Dong, H. Liu, F. Shi, and J. Du, "Prevalence, risk factors, outcomes, and treatment of obstructive sleep apnea in patients with cerebrovascular disease: A systematic review," *J. Stroke Cerebrovas. Dis.*, vol. 27, no. 6, pp. 1471–1480, 2018.

[4] B. Cacho-Díaz, N. A. Lorenzana-Mendoza, H. Spínola-Maroño, G. Reyes-Soto, and C. Cantú-Brito, "Comorbidities, clinical features, and prognostic implications of cancer patients with cerebrovascular disease," *J. Stroke Cerebrovas. Dis.*, vol. 27, no. 2, pp. 365–371, 2018.

[5] U. Mitrović, B. Likar, F. Pernuš, and Ž. Špiclin, "3D–2D registration in endovascular image-guided surgery: Evaluation of state-of-the-art methods on cerebral angiograms," *Int. J. Comput. Assist. Radiol. Surg.*, vol. 13, no. 2, pp. 193–202, 2018.

[6] J. Kim, J. Lee, J. W. Chung, and Y.-G. Shin, "Locally adaptive 2D–3D registration using vascular structure model for liver catheterization," *Comput. Biol. Med.*, vol. 70, pp. 119–130, Mar. 2016.

[7] U. Mitrović, F. Pernuš, B. Likar, and Ž. Špiclin, "Simultaneous 3D–2D image registration and C-arm calibration: Application to endovascular image-guided interventions," *Med. Phys.*, vol. 42, no. 11, pp. 6433–6447, 2015.

[8] S. Matl, R. Brosig, M. Baust, N. Navab, and S. Demirci, "Vascular image registration techniques: A living review," *Med. Image Anal.*, vol. 35, pp. 1–17, Jan. 2017.

[9] S. Miao *et al.*, "Dilated fcn for multi-agent 2D/3D medical image registration," in *Proc. 32nd AAAI Conf. Artif. Intell.*, 2018, pp. 4694–4701.

[10] J. V. Byrne *et al.*, "Assessment of a technique for 2D–3D registration of cerebral intra-arterial angiography," *Brit. J. Radiol.*, vol. 77, no. 914, pp. 123–128, 2004.

[11] S. Demirci, M. Baust, O. Kutter, F. Manstad-Hulaas, H.-H. Eckstein, and N. Navab, "Disocclusion-based 2D–3D registration for aortic interventions," *Comput. Biol. Med.*, vol. 43, no. 4, pp. 312–322, 2013.

[12] J. H. Hipwell *et al.*, "Intensity-based 2-D–3-D registration of cerebral angiograms," *IEEE Trans. Med. Imag.*, vol. 22, no. 11, pp. 1417–1426, Nov. 2003.

[13] J. Feldmar, N. Ayache, and F. Betting, "3D–2D projective registration of free-form curves and surfaces," *Comput. Vis. Image Understand.*, vol. 65, no. 3, pp. 403–424, 1997.

[14] N. Baka, C. T. Metz, C. J. Schultz, R.-J. van Geuns, W. J. Niessen, and T. van Walsum, "Oriented Gaussian mixture models for nonrigid 2D/3D coronary artery registration," *IEEE Trans. Med. Imag.*, vol. 33, no. 5, pp. 1023–1034, May 2014.

[15] J. Feldmar, G. Malandain, N. Ayache, S. Fernández-Vidal, E. Maurincomme, and Y. Trousset, "Matching 3D MR angiography data and 2D X-ray angiograms," in *Proc. Int. Conf. Comput. Vis. Virtual Reality Robot. Med. (CVRMed-MRCAS)*, 1997, pp. 129–138.

[16] P. David, D. Dementhon, R. Duraiswami, and H. Samet, "SoftPOSIT: Simultaneous pose and correspondence determination," *Int. J. Comput. Vis.*, vol. 59, no. 3, pp. 259–284, 2004.

[17] M. Groher, D. Zikic, and N. Navab, "Deformable 2D–3D registration of vascular structures in a one view scenario," *IEEE Trans. Med. Imag.*, vol. 28, no. 6, pp. 847–860, Jun. 2009.

[18] R. A. McLaughlin, J. Hipwell, D. J. Hawkes, J. A. Noble, J. V. Byrne, and T. C. Cox, "A comparison of a similarity-based and a feature-based 2-D–3-D registration method for neurointerventional use," *IEEE Trans. Med. Imag.*, vol. 24, no. 8, pp. 1058–1066, Aug. 2005.

[19] H. Sundar, A. Khamene, C. Xu, F. Sauer, and C. Davatzikos, "A novel 2D-3D registration algorithm for aligning fluoro images with 3D pre-op CT/MR images," in *Proc. Med. Imag. Visualization Image Guid. Procedures Display*, vol. 6141, 2006, Art. no. 61412K.

[20] D. J. Campbell, L. Petersson, L. Kneip, and H. Li, "Globally-optimal inlier set maximisation for camera pose and correspondence estimation," *IEEE Trans. Pattern Anal. Mach. Intell.*, vol. 42, no. 2, pp. 328–342, Feb. 2020.

[21] M. Brown, D. Windridge, and J.-Y. Guillemaut, "Globally optimal 2D-3D registration from points or lines without correspondences," in *Proc. IEEE Int. Conf. Comput. Vis.*, Santiago, Chile, 2015, pp. 2111–2119.

[22] D. Campbell, L. Petersson, L. Kneip, H. Li, and S. Gould, "The alignment of the spheres: Globally-optimal spherical mixture alignment for camera pose estimation," in *Proc. IEEE Conf. Comput. Vis. Pattern Recognit.*, Long Beach, CA, USA, 2019, pp. 11796–11806.

[23] C.-R. Chou, B. Frederick, G. Mageras, S. Chang, and S. Pizer, "2D/3D image registration using regression learning," *Comput. Vis. Image Understand.*, vol. 117, no. 9, pp. 1095–1106, 2013.

[24] H. Liao, W.-A. Lin, J. Zhang, J. Zhang, J. Luo, and S. K. Zhou, "Multiview 2D/3D rigid registration via a point-of-interest network for tracking and triangulation," in *Proc. IEEE Conf. Comput. Vis. Pattern Recognit.*, Long Beach, CA, USA, 2019, pp. 12638–12647.

[25] D. Ruijters, R. Homan, P. Mielekamp, P. Van de Haar, and D. Babic, "Validation of 3D multimodality roadmapping in interventional neuroradiology," *Phys. Med. Biol.*, vol. 56, no. 16, pp. 5335–5354, 2011.

[26] J. Wu, M. Kim, J. Peters, H. Chung, and S. S. Samant, "Evaluation of similarity measures for use in the intensity-based rigid 2D-3D registration for patient positioning in radiotherapy," *Med. Phys.*, vol. 36, no. 12, pp. 5391–5403, 2009.

[27] J. Jomier, E. Bullitt, M. Van Horn, C. Pathak, and S. R. Aylward, "3D/2D model-to-image registration applied to tips surgery," in *Proc. Int. Conf. Med. Image Comput. Comput. Assist. Interv.*, 2006, pp. 662–669.

[28] K.-L. Low, *Linear Least-Squares Optimization for Point-to-Plane ICP Surface Registration*, vol. 4, Univ. North Carolina, Chapel Hill, NC, USA, 2004, pp. 1–3.

[29] M. Groher, T. F. Jakobs, N. Padoy, and N. Navab, "Planning and intraoperative visualization of liver catheterizations: New CTA protocol and 2D-3D registration method," *Acad. Radiol.*, vol. 14, no. 11, pp. 1325–1340, 2007.

[30] Y. Khoo and A. Kapoor, "Non-iterative rigid 2D/3D point-set registration using semidefinite programming," *IEEE Trans. Image Process.*, vol. 25, pp. 2956–2970, 2016.

[31] H. Li and R. Hartley, "The 3D-3D registration problem revisited," in *Proc. IEEE 11th Int. Conf. Comput. Vis.*, Rio de Janeiro, Brazil, 2007, pp. 1–8.

[32] E. B. Van de Kraats, G. P. Penney, D. Tomazevic, T. Van Walsum, and W. J. Niessen, "Standardized evaluation methodology for 2-D–3-D registration," *IEEE Trans. Med. Imag.*, vol. 24, no. 9, pp. 1177–1189, Sep. 2005.

[33] F. Pernus, Ž. Špiclin, B. Likar, and F. Pernuš, "3D-2D registration of cerebral angiograms: A method and evaluation on clinical images," *IEEE Trans. Med. Imag.*, vol. 32, no. 8, pp. 1550–1563, Aug. 2013.

[34] N. Strobel *et al.*, "3D imaging with flat-detector C-arm systems," in *Multislice CT*. Heidelberg, Germany: Springer, 2009, pp. 33–51.

[35] H. Späth, "The cluster dissection and analysis: Theory FORTRAN programs examples," *Math. Comput.*, vol. 47, Oct. 1986, Art. no. 198610.

[36] G. A. Seber, *Multivariate Observations*, vol. 252. New York, NY, USA: Wiley, 2009.